Int J Adv Manuf Technol (2017) 91:2113–2123
DOI 10.1007/s00170-016-9903-7

ORIGINAL ARTICLE

Formation characteristics of the chip and damage equivalent stress of the cutting tool in high-speed intermittent cutting

Xiaobin Cui[1] · **Bo Zhao**[1] · **Feng Jiao**[1] · **Pingmei Ming**[1]

Received: 3 September 2016 / Accepted: 18 December 2016 / Published online: 30 December 2016

Abstract For the purpose of revealing the formation characteristics of the chip and analyzing damage equivalent stress of the cutting tool in high-speed intermittent cutting, cutting tests, and finite element simulation were performed in the present work. Characteristics of chip morphologies acquired in cutting tests were analyzed and compared for different cutting conditions. The effects of cutting parameters on force, temperature, and stress on the shear plane were investigated. On the basis of the concept of damage equivalent stress, the initial damage of the cutting tool and the tool stress were integrated and the influences of cutting parameters on damage equivalent stress were studied. The correlations between damage equivalent stress of the cutting tool and chip formation were analyzed. Analysis results indicated that there existed strong correlations between the evolution of damage equivalent stress of the cutting tool and the chip formation process. Relatively low damage equivalent stress and relatively long tool life appeared at the same time when small values of cutting speed and feed rate were used.

Keywords High-speed cutting · Intermittent cutting · Chip formation · Damage equivalent stress

Nomenclature

v	Cutting speed
f_z	Feed rate
a_p	Axial depth of cut
a_e	Radial depth of cut
N_l	Tool life
$\overline{\sigma}$	Shear stress
T_a	Absolute temperature
$\overline{\varepsilon}$	Shear strain
$\dot{\overline{\varepsilon}}$	Shear strain rate
A	Yield strength
B	Hardening modulus
C	Strain rate sensitivity
n	Strain hardening exponent
m	Thermal softening coefficient
$\dot{\overline{\varepsilon_0}}$	Reference plastic strain
T_{room}	Reference temperature
T_{melt}	Melting temperature
F_{rs}	Resultant cutting forces obtained in simulation
F_{rt}	Resultant cutting forces obtained in cutting tests
F_s	Shear force
T_s	The highest temperature on the shear plane
S_s	The highest Von Mises stress on the shear plane
F_c	Principle cutting force
F_n	Thrust cutting force
ϕ	Shear angle
L	Cutting length
F_{ms}	The maximum value of shear force in the saw-tooth formation process
T_{ms}	The maximum value of the temperature on the shear plane in the saw-tooth formation process
S_{ms}	The maximum value of Von Mises stress on the shear plane in the saw-tooth formation process
σ^*	Damage equivalent stress
$\boldsymbol{\sigma}$	Tri-axial stress imposed on the cutting tool
ν	Poisson's ratio of the tool material
D_{in}	The initial damage of the tool material
P_m	The material porosity
μ	The friction coefficient of the contacting tool material

✉ Bo Zhao
406379340@qq.com

[1] School of Mechanical and Power Engineering, Henan Polytechnic University, Jiaozuo 454003, People's Republic of China

w	Twice the initial microcrack length
d	Verage grain size
σ^*_h	The highest value of damage equivalent stress on the tool body
σ^*_m	The maximum value of damage equivalent stress during the formation of a single saw-tooth
F_r	The maximum resultant cutting force during the formation of a single saw-tooth
T_t	The maximum tool temperature during the formation of a single saw-tooth

1 Introduction

During the high-speed intermittent cutting process, the cutting tools and the workpiece interact with each other. Formation characteristics of the chip reflect the features of the interaction between the tool and the workpiece. The mechanical and thermal loads induced by the interaction have great effects on the fracture of the cutting tool on micro- and macro-scales. It can be deduced that there existed correlations between the characteristics of chip formation and the failure of cutting tool.

The concept of high-speed cutting (HSC) was proposed by Salomon [1] more than 80 years ago. Due to its advantages, HSC technology has been widely used in manufacturing industry [2–4]. With the development of tool materials and machine tools, the cutting speed used by the researchers and the companies keep increasing [5]. Since increasingly high cutting speed is being adopted, much new phenomena and mechanisms during the chip formation process are being continuously discovered. Continuous saw-tooth chip appear when the cutting speed is relatively high. As the cutting speed further increase, separated saw-tooth chip [6–8] arise in the cutting process, which is considered by the investigators [8] as the indicator of ultra-high-speed cutting. The adiabatic shear theory [9, 10] and the cyclic crack theory [11, 12] are the two kinds of theories for the saw-tooth chip formation. Most of the previous studies on chip formation mechanisms concentrated on continuous saw-tooth chip. Relatively few researches [6, 8, 13] were performed to reveal the formation mechanisms of separated saw-tooth chip. High-speed face milling of AISI H13 hardened steel was conducted by Cui and Zhao [6], and it was found that the temperature in the shear band influenced the formation of separated saw-tooth substantially. High-speed orthogonal cutting of Inconel 718 alloy was performed by Su [8] to study the formation mechanisms of chip obtained in different cutting speed ranges. The results indicated that the cyclic crack theory can be used to explain the formation mechanisms of separated saw-tooth. Finite element simulations were conducted by Guo and Yen [13] in order to analyze the formation mechanisms of discontinuous (separated) saw-tooth chip. It was found from the analysis that adiabatic shearing had great effects on the formation of discontinuous saw-tooth in machining of AISI 4340 steel. Previous researches provided much valuable information on chip formation in high-speed cutting. However, it can be concluded that relatively few studies were conducted to investigate the formation mechanisms of separated saw-tooth chip. Quantities such as force, temperature, and stress on the shear plane have great effects on the formation of separated saw-tooth. Scant researches were performed to analyze these quantities.

Previous researches [6, 14, 15] indicated that in high-speed intermittent cutting, the cutting tools were more inclined to fracture due to the relatively severe mechanical and thermal impact. Cui and Zhao [6] investigated the cutting performance of coated carbide tools in high-speed face milling of AISI H13 hardened steel. For different cutting conditions, tool life and tool wear mechanisms were analyzed and compared. Zhao and Ai [14] studied the fabrication and cutting performance of an Al_2O_3–(W,Ti) C functionally gradient ceramic tool in intermittent cutting. It was found that when the cutting speed was relatively low, the functionally gradient ceramic tool and homogeneous ceramic tool shared similar failure modes. However, as the cutting speed increased, they have different failure modes. Ultra-high-speed face milling was performed by Liu et al. [15] to investigate the wear patterns and mechanisms of cutting tools. The analysis results indicated that as the combination of cutting tool and workpiece changed, the tool wear types varied. It can be found that past studies on tool failure mainly focused on the analysis of the morphologies of the failed tool. Few researches were conducted with the initial state of the cutting tool considered. The cutting tools with certain initial state fails because of the combined effects of mechanical and thermal loads. Therefore, the effects of the tool's initial state and the external loads should be integrated in the analysis of tool failure.

High-speed intermittent cutting tests and finite element simulation are conducted in the present work. Characteristics of chip morphologies obtained in the tests are investigated for different cutting conditions. The features of separated saw-tooth acquired at different cutting speeds are analyzed and compared. The effects of cutting parameters on force, temperature, and stress on the shear plane are studied on the basis of finite element simulation. The initial damage of the cutting tool and the tool stress are integrated based on the concept of damage equivalent stress. The influences of cutting parameters on damage equivalent stress are analyzed. The correlations between chip formation process and damage equivalent stress of the cutting tool are investigated. Damage equivalent stress and tool lives acquired at different combinations of cutting parameters are compared and the relationship between them is identified.

2 Experimental procedures and finite element simulation

2.1 Experimental procedures

Tool holder which has a diameter of 80 mm was used in the cutting tests. Only one of the teeth was utilized in order to eliminate the effects of tool tip run out on tool wear [16]. Tungsten carbide inserts were used in the present work. The tool angles have great effects on chip formation and cutting forces. Taking the cutting conditions into consideration, the tool company recommended the tool angles adopted in the study. In the present work, the rake angle and clearance angle of the cutting tool were −8° and 8°, respectively. AISI H13 hardened steed (46~47HRC) was applied as the workpiece. Table 1 shows the chemical composition of the workpiece. All of the cutting tests were performed on a machining center with a maximum spindle rotation speed of 10,000 rpm.

For all the cutting tests, symmetric milling was used. Cutting speed v (600, 1000, 1400, 1800, and 2200 m/min) utilized in the milling tests was in the range of 600 to 2200 m/min at an interval of 400 m/min. Feed rate f_z (0.02, 0.04, 0.06, 0.08, and 0.10 mm/tooth) ranging from 0.02 to 0.10 mm/tooth was used. Axial depth of cut a_p and radial depth of cut a_e were fixed as 0.4 and 5 mm, respectively. All of the cutting tests were carried out under dry conditions. Each trial was replicated three times. The cutting forces were measured by means of a Kistler piezoelectric dynamometer (type 9257B) during the milling tests as shown in Fig. 1. The dynamometer was mounted on the machine table and the charge generated at the dynamometer was amplified using a multichannel charge amplifier. A low-pass filter was used at the charge amplifier for removing noise induced by process variables. The sampling frequency of the data was 10,000 Hz. A digital microscope was used to examine the tool flank wear periodically. When the tool flank wear reached or increased over 0.3 mm, tool life N_l was recorded using the number of cutting cycles. When the milling tests were finished, the chip morphologies were observed by means of a Keyence VHX-600E 3D digital microscope with a large depth of field.

2.2 Finite element simulation

Abaqus/Explicit software was applied in the simulation of cutting process to analyze quantities difficult to measure directly in the tests. Analysis of the recorded cutting forces indicated that cutting force in z direction was relatively low and much smaller than forces in x and y directions. This means that the interactions between the cutting tool and the workpiece mainly happened in x and y directions. Therefore, the cutting process was modeled to be two-dimensional. The schematic of finite element simulation was shown in Fig. 2. The workpiece was modeled as elastic–plastic material and the cutting tool was set to be elastic. Table 2 presents the material properties of the workpiece and the cutting tool. The boundary conditions in the simulation were consistent with those in the cutting tests.

It is of great importance to select a suitable material-constitutive model for the workpiece. The effects of strain, strain rate, stress, and temperature should all be incorporated in the model so that the cutting process can be simulated successfully. In the present work, Johnson and Cook constitutive model was used and it can be defined as follows:

$$\overline{\sigma} = \left[A + \mathrm{B}\left(\overline{\varepsilon}\right)^{n}\right]\left[1 + \mathrm{Cln}\left(\frac{\dot{\overline{\varepsilon}}}{\dot{\overline{\varepsilon_0}}}\right)\right]\left[1\text{-}\left(\frac{T_\mathrm{a}-T_\mathrm{room}}{T_\mathrm{melt}-T_\mathrm{room}}\right)^{m}\right] \tag{1}$$

where $\overline{\sigma}$, T_a, $\overline{\varepsilon}$, and $\dot{\overline{\varepsilon}}$ are shear stress, absolute temperature, shear strain, and shear strain rate, respectively. The material behaviors are substantially influenced by the yield strength A, the hardening modulus B, the strain rate sensitivity C, the strain hardening exponent n, the thermal softening coefficient m, the reference plastic strain $\dot{\overline{\varepsilon_0}}$, the reference temperature T_{room}, and the melting temperature T_{melt}. Based on the work by Umer [17], these critical parameters were set as A = 674.8 MPa, B = 239.2 MPa, C = 0.056, n = 0.44, and m = 2.7.

3 Results and discussion

3.1 Chip formation

Chip morphologies obtained at different combinations of cutting parameters were analyzed and compared. It was found that even though different values of feed rate were adopted, chip morphologies evolved in similar way as cutting speed increased. Figure 3 shows the typical morphologies of the chip obtained at different cutting speeds. It can be seen from Fig. 3 that when cutting speed increased, the degree of chip serration became larger. It should be noted that separated saw-tooth

Table 1 Chemical composition of AISI H13 tool steel (wt.%)

C	Mn	Si	Cr	Mo	V	Ni	Fe
0.32–0.45	0.20–0.50	0.80–1.2	4.75–5.50	1.10–1.75	0.80–1.20	0–0.30	Bal.

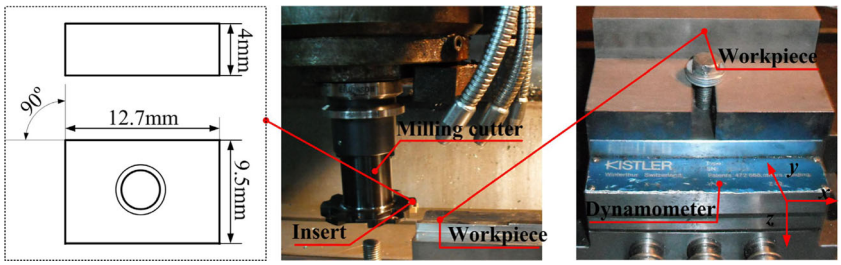

Fig. 1 Experimental setup

chip started to form at the cutting speed of 1800 m/min. Therefore, the cutting speed of 1800 m/min can be considered as a transition speed. It was observed that all the serrated chip were separated at the cutting speed of 2200 m/min.

It was found that though the separated saw-tooth appeared at cutting speeds of 1800 and 2200 m/min, the saw-tooth exhibited varying characteristics at different cutting speeds. Figure 4 shows the typical morphologies of the separated saw-tooth obtained at cutting speeds of 1800 and 2200 m/min. It can be seen from Fig. 4 that the separated saw-tooth can be divided into two regions A and B. Region A exhibited the features of steel which had been subjected to high temperature heating. Comparisons between Fig. 4c and d indicate that the edges of region B were relatively smooth at cutting speeds of 1800 and 2200 m/min. The area of region B changed little as cutting speed increased. However, it can be found that the edges of region A evolved to be irregular as cutting speed increased from 1800 to 2200 m/min. It can also be seen that the area of region A became much larger when cutting speed increased to be 2200 m/min. It is inferred that higher cutting temperature arose at higher cutting speed. The evolutions of shape and area of region A with the increase of cutting speed were substantially influenced by the higher cutting temperature. Due to the higher temperature in the chip formation process, larger area of the saw-tooth endured high temperature heating and had lower strength, leading to larger area of region A at higher cutting speed. Because of the lower strength and larger area in region A, saw-tooth of the chip was separated more easily and randomly, resulting in the irregular edge of region A at the cutting speed of 2200 m/min.

For the purpose of analyzing the evolutions of several critical quantities such as force, temperature, and stress during the chip formation process, finite element simulation of the cutting process was conducted. Comparisons between the resultant cutting forces obtained in simulation (F_{rs}) and cutting tests (F_{rt}) were conducted to validate the correctness of the simulation as shown in Fig. 5. Deviation D_e is introduced to represent the difference between F_{rs} and F_{rt}. D_e can be obtained using the following equation:

$$D_e = \frac{F_{rs} - F_{rt}}{F_{rt}} \cdot 100\% \tag{2}$$

It can be observed from Fig. 5 that there existed relatively small differences between F_{rs} and F_{rt} for different cutting parameter combinations, which demonstrated the correctness of the simulation to some extent.

The development of shear force F_s, the highest temperature T_s, and the highest Von Mises stress S_s on the shear plane (Fig. 6a) were analyzed based on the simulated results. F_s can be acquired based on Eq. (2):

$$F_s = F_c \cdot \cos\phi - F_n \cdot \sin\phi \tag{2}$$

where F_c is the principle cutting force and F_n is the thrust cutting force and ϕ is the shear angle. F_c, F_n, and ϕ can be obtained in the simulation. Figure 6b–d shows the typical developing processes of F_s, T_s, and S_s with cutting length L during the formation of a single saw-tooth. It can be observed that as the cutting length grew larger, the values of F_s, T_s, and

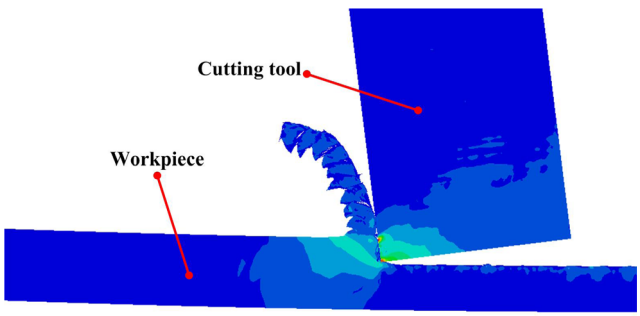

Fig. 2 Schematic of finite element simulation

Table 2 Material properties of the workpiece and the cutting tool

Material properties	Workpiece	Cutting tool
Density (kg m^{-3})	7.72×10^3	14.5×10^3
Young's modulus (Pa)	2.12×10^{11}	6.24×10^{11}
Thermal conductivity (W m^{-1} K^{-1})	28.5	81
Heat capacity (J kg^{-1} K^{-1})	565	410
Thermal expansion (K^{-1})	9.6×10^{-6}	5.3×10^{-6}

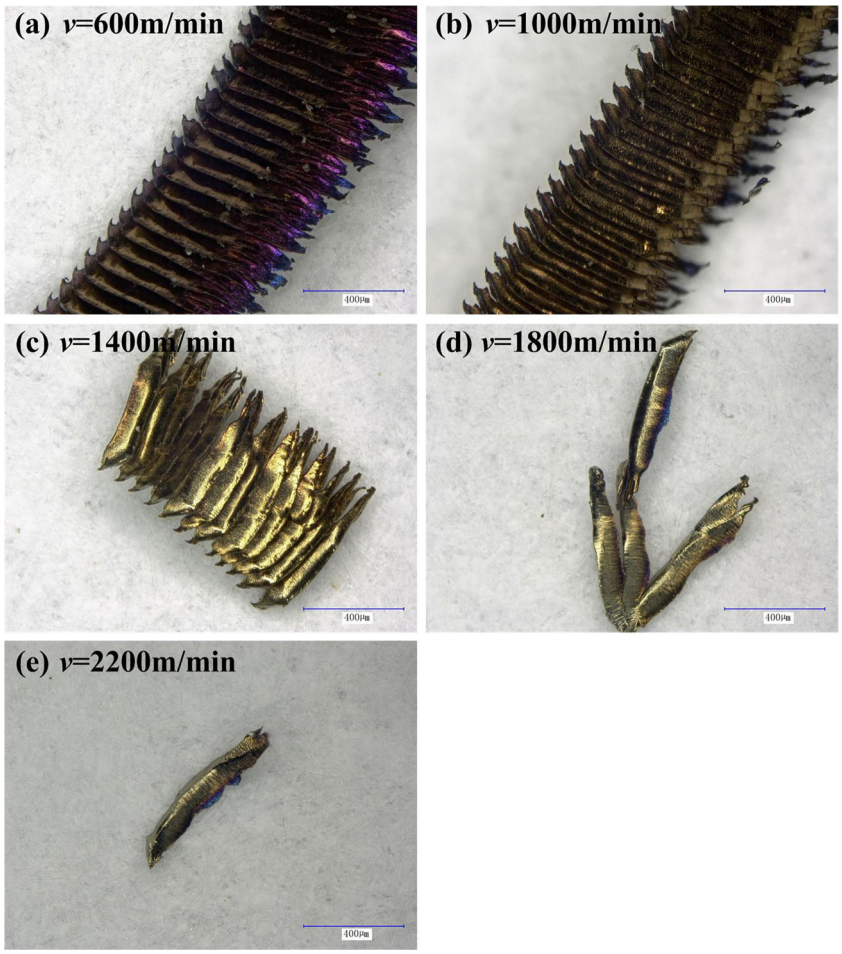

Fig. 3 Typical morphologies of the chip obtained at different cutting speeds (f_z = 0.04 mm/tooth, a_p = 0.4 mm, a_e = 5 mm)

S_s increased first and then decreased. It can be seen from Fig. 6b, c that the maximum values of F_s and T_s in the saw-tooth formation process were represented by F_{ms} and T_{ms}, respectively. The maximum value of S_s was denoted as S_{ms}

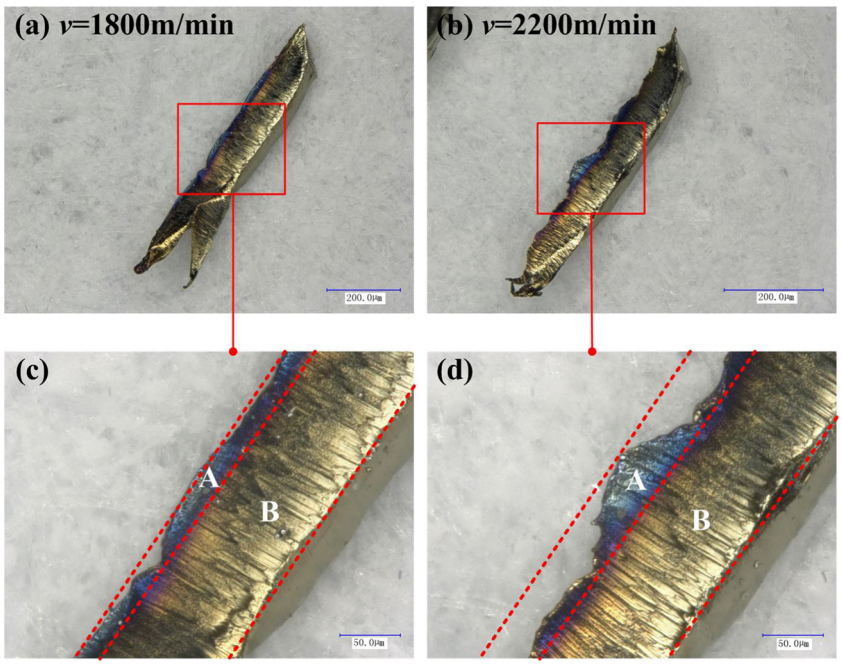

Fig. 4 Typical morphologies of the separated saw-tooth obtained at cutting speeds of 1800 and 2200 m/min (f_z = 0.04 mm/tooth, a_p = 0.4 mm, a_e = 5 mm)

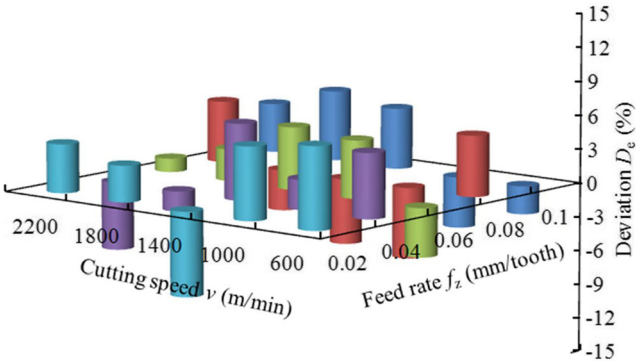

Fig. 5 Comparisons between the resultant cutting forces obtained in simulation (F_{rs}) and cutting tests (F_{rt}) (a_p = 0.4 mm, a_e = 5 mm). **a** Shear plane captured in the simulation. **b** Development of F_s with cutting length L. **c** Development of T_s with cutting length L. **d** Development of S_s with cutting length L

as shown in Fig. 6d. It was found that F_{ms}, T_{ms}, and S_{ms} arose approximately at the same cutting length L_m. Analysis of F_{ms}, T_{ms}, and S_{ms} were concentrated on in the present work.

3.2 Force, temperature, and stress during chip formation

F_{ms}, T_{ms}, and S_{ms} were obtained and investigated for different combinations of cutting parameters. Figure 7 shows the typical evolutions of F_{ms}, T_{ms}, and S_{ms} with cutting speed. It can be found from Fig. 7 that F_{ms}, T_{ms}, and S_{ms} exhibited varying evolving trends with the increase of cutting speed. It can be seen from Fig. 7a that F_{ms} decreased as the cutting speed became higher. Figure 7b indicates that the value of T_{ms} became larger as the cutting speed increased. This validated the inference that higher cutting temperature appeared at higher cutting speed. It was found that the values of T_{ms} increased to be close to the melting point (1427 °C) of the workpiece when cutting speed was no less than the transition cutting speed of 1800 m/min. Taking the evolution of chip morphology with cutting speed into account, it can be inferred that the occurrence of high temperature influenced the formation of separated saw-tooth greatly. With the thermal softening effect considered, it can be deduced that the increasing trend of temperature T_{ms} with cutting speed shown in Fig. 7b had great influence on the decreasing trend of F_{ms} presented in Fig. 7a. It can be observed from Fig. 7c that when the cutting speed increased, the value of S_{ms} became smaller. This phenomenon can be attributed to the lower yield strength of the workpiece at higher temperature.

Figures 8 and 9 show the fitted curved surfaces for F_{ms} and T_{ms} obtained at different combinations of cutting parameters, respectively. The fitted curved surface for S_{ms} is shown in Fig. 10. It can be seen from Fig. 8 that relatively small value of F_{ms} arose when relatively low feed rate and relatively high cutting speed were adopted. It can also be found that when relatively high feed rate and relatively low cutting speed were used, the largest value of F_{ms} appeared. Figure 9 indicates that

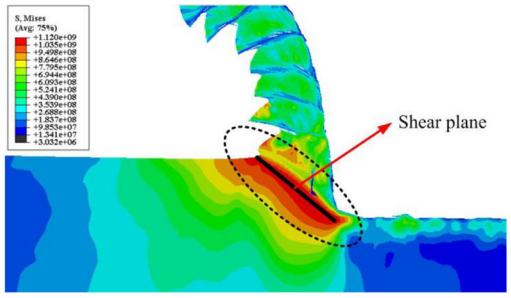

(a) Shear plane captured in the simulation

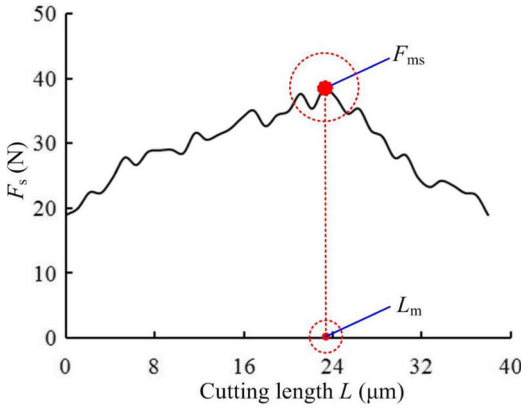

(b) Development of F_s with cutting length L

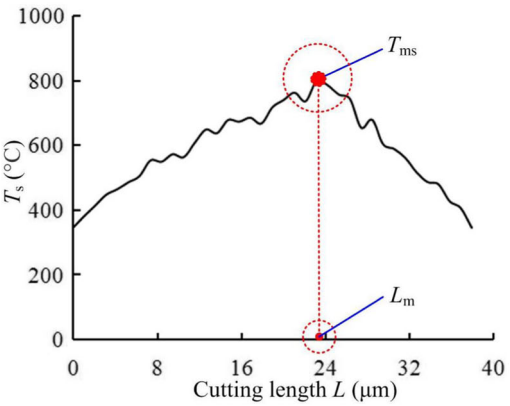

(c) Development of T_s with cutting length L

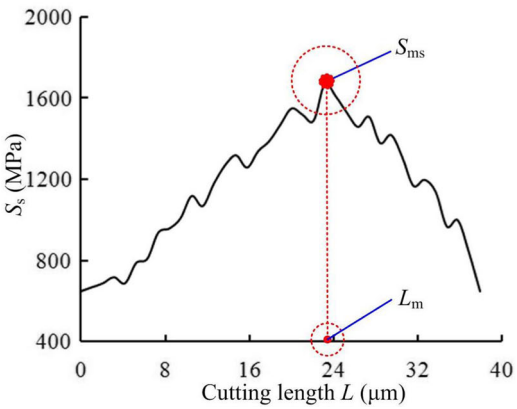

(d) Development of S_s with cutting length L

◀ **Fig. 6** The typical development of F_s, T_s, and S_s with cutting length L during the formation of a single saw-tooth (v = 1000 m/min, f_z = 0.04 mm/tooth, a_p = 0.4 mm, a_e = 5 mm). **a** The typical evolution of F_{ms} with cutting speed v. **b** The typical evolution of T_{ms} with cutting speed v. **c** The typical evolution of S_{ms} with cutting speed v

when higher feed rate and cutting speed were utilized, larger value of T_{ms} arose. The smallest value of T_{ms} can be acquired when the lowest feed rate and cutting speed were applied. It should be pointed out that though T_{ms} grew larger as feed rate increased, the growth rate was low. It can be found from Fig. 10 that the developing trend of S_{ms} with feed rate or cutting speed was similar to that of F_{ms}. The utilization of relatively low feed rate and relatively high cutting speed led to relatively small value of S_{ms}.

3.3 Damage equivalent stress of the cutting tool

The initial state of the tool material and the tool stress can be integrated by the concept of damage equivalent stress [18]. Damage equivalent stress can be applied to analyze the rupture of brittle and quasi-brittle materials [19]. Damage equivalent stress σ^* [19] of the cutting tool can be expressed as follows:

$$\sigma^* = \left\{ (1+\nu)\langle\boldsymbol{\sigma}\rangle^+ : \langle\boldsymbol{\sigma}\rangle^+ - \nu\langle \mathrm{tr}\sigma\rangle^2 + \frac{1-D_{in}}{1-hD_{in}}\left[(1+\nu)\langle\boldsymbol{\sigma}\rangle^- : \langle\boldsymbol{\sigma}\rangle^- - \nu\langle -\mathrm{tr}\sigma\rangle^2\right]\right\}^{1/2} \tag{3}$$

where $\boldsymbol{\sigma}$ is the tri-axial stress imposed on the cutting tool and it can be obtained through simulation, ν is Poisson's ratio of the tool material under consideration and it was acquired as 0.22, h is usually on the order of 0.2, and D_{in} is the initial damage of the tool material. Based on the previous work [18], the initial state of the tool material was evaluated using initial damage D_{in} and it can be expressed as follows:

$$D_{in} = \frac{4P_m\mu\sin^2\theta(\kappa+1)(\nu+1)\left[\sin\theta\cos\theta-\mu\sin^2\theta\right]\left(w\sin\frac{\pi l^*}{w}\right)^{-1/2}\left(2\pi l^{**}\right)^{1/2}}{2+4P_m\mu\sin^2\theta(\kappa+1)(\nu+1)\left(\sin\theta\cos\theta-\mu\sin^2\theta\right)\left(w\sin\frac{\pi l^*}{w}\right)^{-1/2}\left(2\pi l^{**}\right)^{1/2}} \tag{4}$$

For the purpose of acquiring the value of D_{in}, some important parameters in Eq. (4) should be determined. In Eq. (4), P_m is the material porosity and it was obtained as 0.019. μ is the friction coefficient of the contacting tool material and its value was found to be 0.47. The value of angle θ can be considered as $\pi/4$[18]. Parameter κ can be calculated using equation $\kappa = [(3-\nu)/(1+\nu)]$. According to the work conducted by Kemeny [20], the value of w was twice the initial microcrack length and the crack length was considered to be the size of the tool material grain. The average grain size (d) of the tool material was obtained as 1.64 μm. The values of l^* and l^{**} can be acquired using equations $l^* = 0.135d$ [21] and

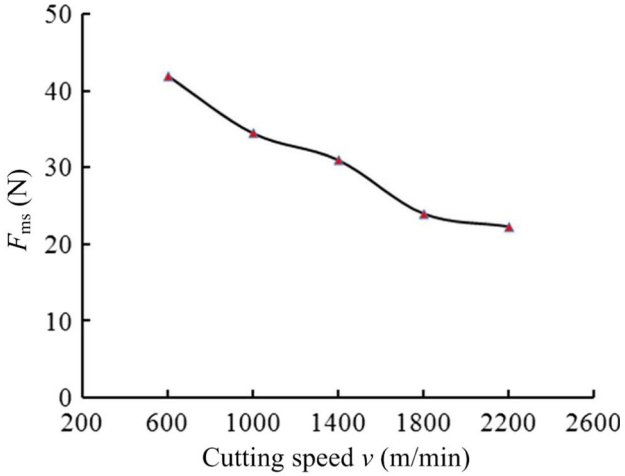

(a) The typical evolution of F_{ms} with cutting speed v

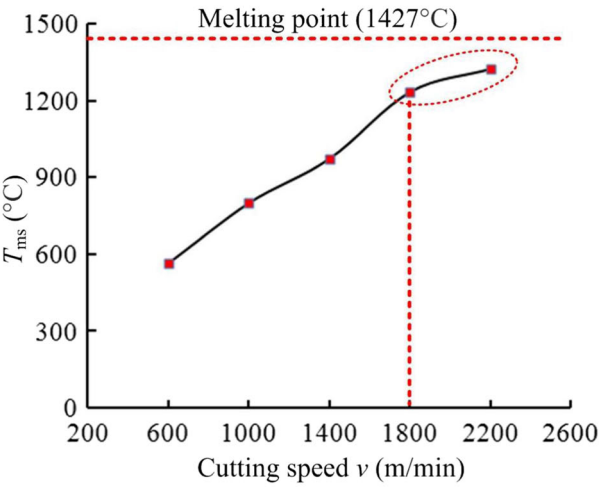

(b) The typical evolution of T_{ms} with cutting speed v

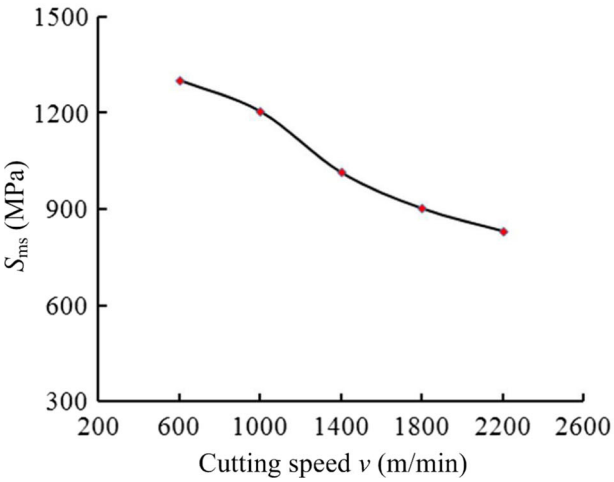

(c) The typical evolution of S_{ms} with cutting speed v

Fig. 7 The typical evolutions of F_{ms}, T_{ms}, and S_{ms} with cutting speed v (f_z = 0.04 mm/tooth, a_p = 0.4 mm, a_e = 5 mm)

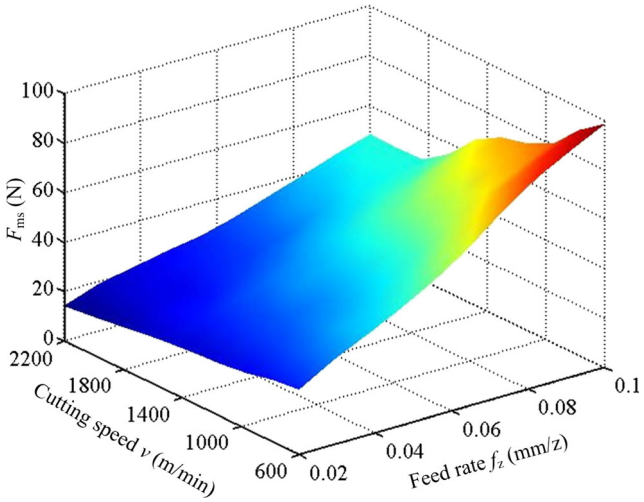

Fig. 8 The fitted curved surface for F_{ms} obtained at different combinations of cutting parameters (a_p = 0.4 mm, a_e = 5 mm)

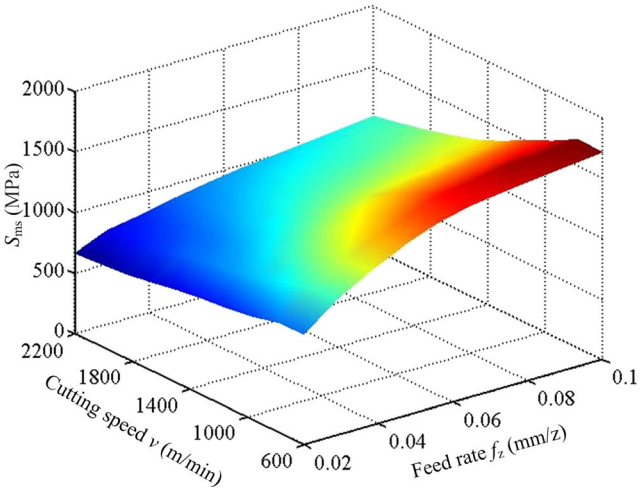

Fig. 10 The fitted curved surface for S_{ms} obtained at different combinations of cutting parameters (a_p = 0.4 mm, a_e = 5 mm)

$l^{**} = 0.0415d$ [22], respectively. On the basis of Eq. (4), the initial damage D_{in} of the tungsten carbide tool material under consideration was found to be 0.0074.

The highest value of σ^* on the tool body was represented by σ^*_h. Figure 11 shows the typical evolution of σ^*_h with cutting length during the formation of a single saw-tooth. It can be seen from Fig. 11 that σ^*_h increased first and then decreased as cutting length increased. The evolving processes of F_s, T_s, and S_s during the formation of a single saw-tooth were presented in Fig. 6. Comparisons between Figs. 11 and 6 were made, and it can be observed that the evolving trend of σ^*_h was similar to those of F_s, T_s, and S_s. It can be inferred from Eq. (3) that the value of σ^*_h was closely related to the stress on the cutting tool. Relatively high cutting temperature usually leads to relatively large temperature gradient in the cutting tool, which subsequently contribute to the increase of tool stress. The evolution of T_s reflected the changes of cutting temperature. Therefore, higher value of T_s was beneficial to the increase of σ^*_h and it was possible that σ^*_h have the same variation trend with T_s. The maximum value of σ^*_h during the formation of a single saw-tooth was represented by σ^*_m. The cutting length at which σ^*_m arose was the same as the length L_m where F_{ms}, T_{ms}, and S_{ms} appeared. The frequencies relating to the evolutions of F_s, T_s, S_s, and σ^*_h in the chip formation process were calculated and compared. It was found that when the combination of cutting parameters was fixed, these frequencies have the same value as the frequency f of the saw-tooth formation. Figure 12 shows the typical development of frequency f with cutting speed. It can be observed from Fig. 12 that frequency f increased with cutting speed. However, the rate of growth became lower when the cutting speed became higher. It can be found from the discussions above that there existed strong correlations between the evolution of damage

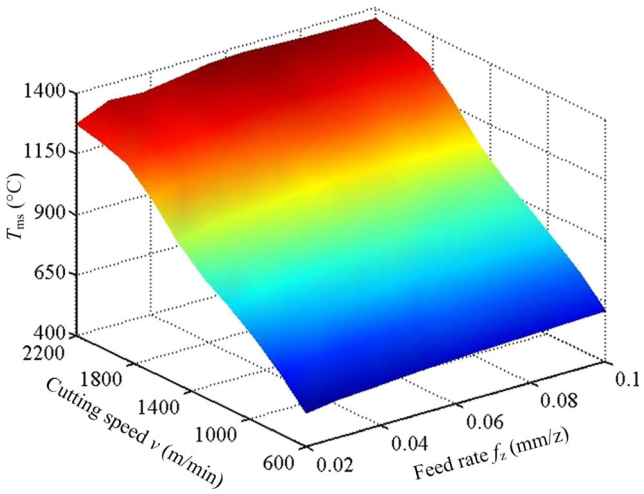

Fig. 9 The fitted curved surface for T_{ms} obtained at different combinations of cutting parameters (a_p = 0.4 mm, a_e = 5 mm)

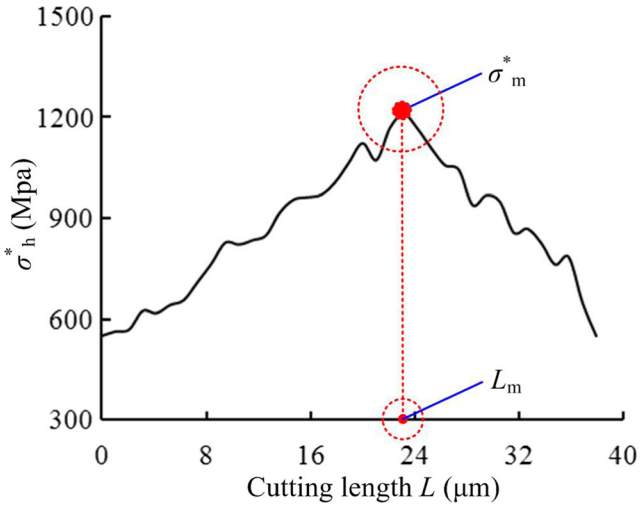

Fig. 11 The typical evolution of σ^*_h with cutting length L during the formation of a single saw-tooth (v = 1000 m/min, f_z = 0.04 mm/tooth, a_p = 0.4 mm, a_e = 5 mm)

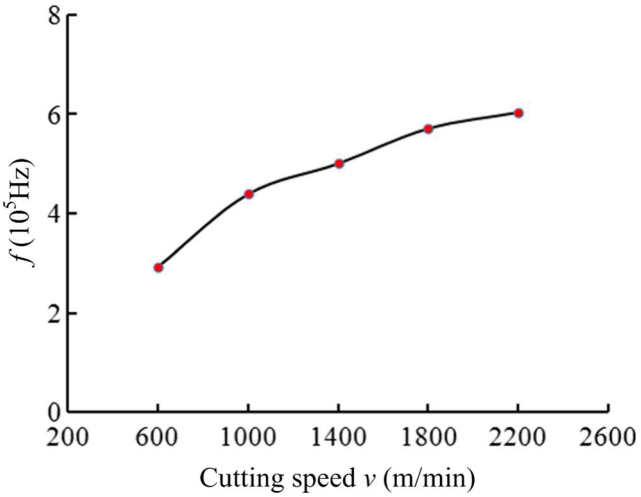

Fig. 12 The typical development of frequency f with cutting speed (f_z = 0.04 mm/tooth, a_p = 0.4 mm, a_e = 5 mm)

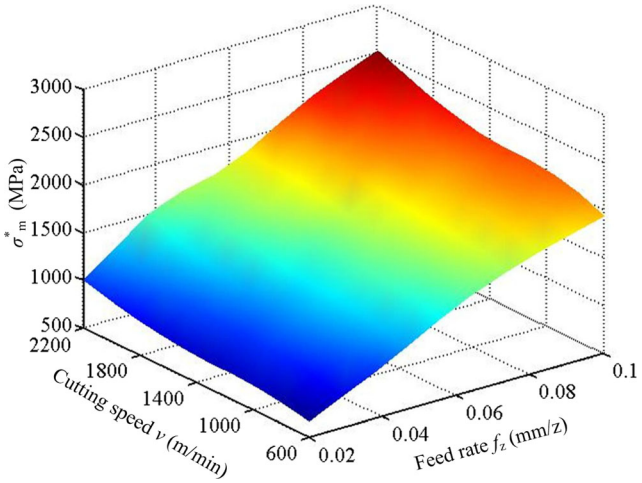

Fig. 14 The fitted curved surfaces for σ^*_m obtained at different combinations of cutting parameters (a_p = 0.4 mm, a_e = 5 mm)

equivalent stress of the cutting tool and the chip formation process. It should be noted that damage equivalent stress of the cutting tool did not have direct influences on the chip formation process. Damage equivalent stress greatly influenced the microscopic and macroscopic fracture of the cutting tool. Due to the effects induced by damage equivalent stress, the macroscopic fracture might arise on the cutting tool and the tool geometry changed. The changes of tool geometry altered the interaction between the cutting tool and the workpiece and subsequently influenced the formation process of chip.

Analyses of the maximum resultant cutting force F_r and the maximum tool temperature T_t during the formation of a single saw-tooth were conducted. The analysis results indicated that when cutting speed increased, the evolving trends of F_r and T_t were similar to F_{ms} and T_{ms}, respectively. Figure 13 shows the typical evolution of σ^*_m with cutting speed. It can be observed from Fig. 13 that σ^*_m kept increasing as the cutting speed increased. It can be found that the developing trend of σ^*_m was different from that of S_{ms} shown in Fig. 7c. Figure 13 indicates that when cutting speed was higher than the transition value of 1800 m/min, σ^*_m grew faster as cutting speed increased. Since cutting force F_r decreased when cutting speed became higher, the increase of σ^*_m with cutting speed can be attributed to the higher tool temperature and higher degree of chip serration. σ^*_m was substantially influenced by the tool stress. Due to the higher tool temperature, the temperature gradient in the cutting tool was greater, leading to larger thermal stress. Because of the higher degree of chip serration, greater mechanical and thermal impact was imposed on the cutting tool [23], resulting in that higher tool stress was inclined to arose in the cutting process.

Figures 14 and 15 present the fitted curved surfaces for σ^*_m and N_l obtained at different cutting parameter combinations. It can be observed from Figs. 14 and 15 that lower value of σ^*_m

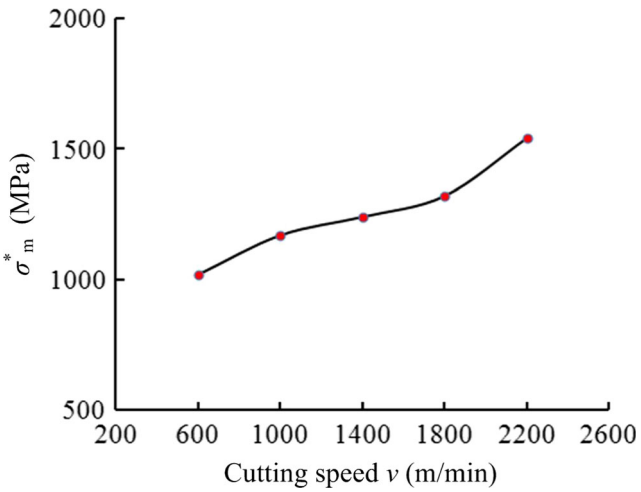

Fig. 13 The typical evolution of σ^*_m with cutting speed (f_z = 0.04 mm/tooth, a_p = 0.4 mm, a_e = 5 mm)

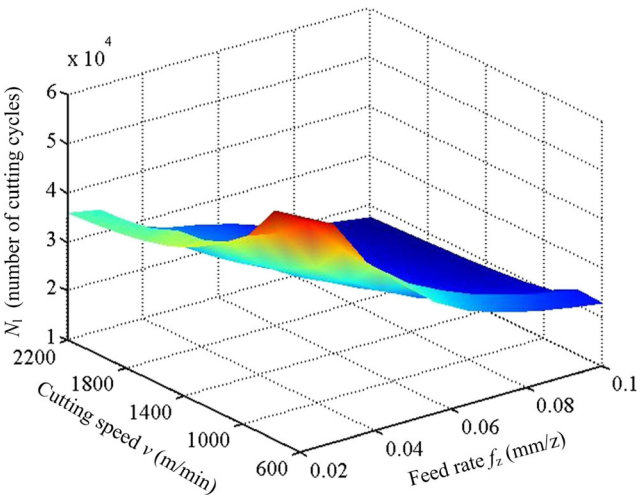

Fig. 15 The fitted curved surfaces for N_l obtained at different combinations of cutting parameters (a_p = 0.4 mm, a_e = 5 mm)

was always accompanied by longer tool life N_l. It can be seen from Fig. 14 that when relatively small values of cutting speed and feed rate were adopted, the lowest value of σ^*_m and the highest value N_l can be obtained at the same time. Comparisons between Figs. 10 and 14 were conducted and it can be found that evolving trend of σ^*_m was opposite to that of S_{ms} as cutting parameters changed.

4 Conclusions

The following conclusions can be drawn from the present work:

- The separated saw-tooth chip began to arise at the transition cutting speed of 1800 m/min, and it can be divided into two regions A and B. Region A exhibited the features of steel which had been heated at high temperature. The edges of region A changed to be irregular and the area of region A became larger as cutting speed increased from 1800 to 2200 m/min. The evolutions of shape and area of region A with cutting speed were greatly influenced by the higher cutting temperature at higher cutting speed. In the formation process of a single saw-tooth, the values of shear force F_s, the highest temperature T_s, and the highest Von Mises stress S_s on the shear plane increased first and then decreased as the cutting length grew larger. The maximum values of F_s (F_{ms}), T_s (T_{ms}), and S_s (S_{ms}) in the saw-tooth formation process appeared at the same cutting length L_m.
- The appearance of high temperature at the cutting speeds of 1800 and 2200 m/min influenced the formation of separated saw-tooth substantially. Relatively small value of F_{ms} arose when relatively low feed rate and relatively high cutting speed were used. The smallest value of T_{ms} can be obtained when the lowest feed rate and cutting speed were adopted. The use of relatively low feed rate and relatively high cutting speed resulted in relatively small value of S_{ms}.
- The initial damage D_{in} of the tool material was obtained as 0.0074. Compared to F_s, T_s, and S_s, the highest value σ^*_h of damage equivalent stress on the tool body evolved in a similar way as cutting length increased. The maximum value of σ^*_h (σ^*_m) during the formation of a single saw-tooth arose at the cutting length L_m where F_{ms}, T_{ms}, and S_{ms} appeared. The evolving frequencies of F_s, T_s, S_s, and σ^*_h were the same as the saw-tooth formation frequency f. When relatively small values of cutting speed and feed rate were adopted, the lowest σ^*_m and the longest N_l appeared at the same time.

Acknowledgments This project is supported by National Natural Science Foundation of China (Grant No. 51505132 and Grant No. 51475148), China Postdoctoral Science Foundation (Grant No. 2016T90666 and Grant No. 2015M580628) and Program for Science & Technology Innovation Team in Universities of Henan Province (15IRTSTHN013).

References

1. Salomon CJ (1931) Process for machining metals of similar acting materials when being worked by cutting tools. German patent, Number 523594
2. Toh CK (2006) Cutter path orientations when high-speed finish milling inclined hardened steel. Int J Adv Manuf Technol 27(5–6):473–480
3. Cui X, Zhao J, Dong Y (2013) The effects of cutting parameters on tool life and wear mechanisms of CBN tool in high-speed face milling of hardened steel. Int J Adv Manuf Technol 66(5–8):955–964
4. Zheng G, Zhao J, Zhou Y, Li A, Cui X, Tian X (2013) Performance of graded nano-composite ceramic tools in ultra-high-speed milling of Inconel 718. Int J Adv Manuf Technol 67(9–12):2799–2810
5. Cui X, Zhao J, Tian X (2012) Tool wear in high-speed face milling of AISI H13 steel. Proc Inst Mech Eng B J Eng Manuf 226(10):1684–1693
6. Cui X, Zhao J (2014) Cutting performance of coated carbide tools in high-speed face milling of AISI H13 hardened steel. Int J Adv Manuf Technol 71(9–12):1811–1824
7. Liu ZQ, Su GS (2012) Characteristics of chip evolution with elevating cutting speed from low to very high. Int J Mach Tools Manuf 54–55:82–85
8. Su GS (2011) Evolution and mechanisms of saw-tooth chip formation in high-speed machining. Ph.D. thesis, Shandong University, Jinan
9. Ye GG, Xue SF, Ma W, Jiang MQ, Ling Z, Tong XH, Dai LH (2012) Cutting AISI 1045 steel at very high speeds. Int J Mach Tools Manuf 56:1–9
10. Molinari A, Musquar C, Sutter G (2002) Adiabatic shear banding in high speed machining of Ti–6Al–4V: experiments and modeling. Int J Plast 18(4):443–459
11. Vyas A, Shaw MC (1999) Mechanics of saw-tooth chip formation in metal cutting. J Manuf Sci Eng Trans ASME 121(2):163–172
12. Shaw MC, Vyas A (1993) Chip formation in the machining of hardened steel. CIRP Ann 42(1):29–33
13. Guo YB, Yen DW (2004) A FEM study on mechanisms of discontinuous chip formation in hard machining. J Mater Process Technol 155–156:1350–1356
14. Zhao J, Ai X (2006) Fabrication and cutting performance of an Al_2O_3–(W,Ti) C functionally gradient ceramic tool. Int J Mach Mach Mater 1(3):277–286
15. Liu ZQ, Ai X, Zhang H, Wang ZT, Wan Y (2002) Wear patterns and mechanisms of cutting tools in high-speed face milling. J Mater Process Technol 129(1–3):222–226
16. Zhang S, Li JF, Wang YW (2012) Tool life and cutting forces in end milling Inconel 718 under dry and minimum quantity cooling lubrication cutting conditions. J Clean Prod 32:81–87
17. Umer U (2012) High speed turning of H-13 tool steel using ceramics and PCBN. J Mater Eng Perform 21(9):1857–1861
18. Cui X, Wang D, Guo J (2016) Performance optimization for cemented carbide tool in high-speed milling of hardened steel with initial microstructure considered. Int J Mech Sci 114:52–59
19. Lemaitre J, Desmorat R (2005) Engineering damage mechanics: ductile, creep, fatigue and brittle failures. Springer, Berlin
20. Kemeny JM (1991) A model for non-linear rock deformation under compression due to sub-critical growth. Int J Rock Mech Min Sci Geomech Abstr 28(6):459–467

21. Horii H, Nemat-Nasser S (1986) Brittle failure in compression: splitting, faulting, and brittle-ductile transition. Philos Trans R Soc A Math Phys Eng Sci 319:337–374
22. Nemat-Nasser S, Obata M (1988) A microcrack model of dilatancy in brittle materials. J Appl Mech 55(1):24–35
23. Cui X, Zhao B, Jiao F, Zheng J (2016) Chip formation and its effects on cutting force, tool temperature, tool stress, and cutting edge wear in high-and ultra-high-speed milling. Int J Adv Manuf Technol 83(1–4):55–65